Atmos. Meas. Tech. Discuss., 6, C4338–C4350, 2014
www.atmos-meas-tech-discuss.net/6/C4338/2014/

Atmospheric Measurement Techniques Discussions

Interactive comment on "Towards higher accuracy and better frequency response with standard multi-hole probes in turbulence measurement with Remotely Piloted Aircraft (RPA)" *by* N. Wildmann et al.

N. Wildmann et al.

norman.wildmann@uni-tuebingen.de

Received and published: 11 February 2014

Many thanks for the detailed review. In the following I will comment on each point. The referee comments will be repeated in italic before the answer.

Full Screen / Esc

Printer-friendly Version

Interactive Discussion

Discussion Paper

General remarks

We agree that aerodynamic flight effects play a role for the airborne wind measurement with multi-hole probes. The focus in the article that we present is the airflow measurement by the probe itself, which is a crucial part of the wind calculation. We showed a number of critical issues that we believe deserve careful revision in every airborne turbulence probe. We did provide field measurements in flight to show the performance of the flow probe setup in practice. We consciously did not present wind measurements, in order to have a raw view on the flow probe performance and not have to interpret possible errors introduced by the inertial measurement unit. A future study is planned, which will deal with the aerodynamic effects, the inertial measurement system and general wind measurement uncertainties for the MASC system.

1 Specific comments

1. *Page 9789, lines 18-20: This method of using only the five holes should be described in more details. In Fig. 5 the static (barometric) pressure is shown to be measured, but in which position on the aircraft. Static pressure defect may get quite significant depending on the measurement positions.*
   The definition of the dimensionless coefficient k_p in table 1 contains an error. It should be:

$$\frac{P_s + \Delta P - p}{dP_0 - \Delta P} \tag{1}$$

   The static pressure measurement is calibrated and corrected with five hole probe measurements. The position where P_s is measured is thus not important, since barometric pressure is calibrated with respect to ΔP and the angle of the probe.

AMTD
6, C4338–C4350, 2014

If there is a pressure defect at the position where P_s is measured, this will also affect the low pressure port of the transducers measuring dP_i and the defect will cancel out (see figure 5 in the manuscript). It only needs to be ensured that the difference between the common low pressure port and the maximum expected pressure at the probe tip does not exceed the measuring range of the transducers.

2. *Page 9789, line 21: "Figure ?? shows ..." should probably be "Figures 7 and 8 show... in wind tunnel and one flight leg of 1000 m (excluding bends), respectively.. ". Some discussion on Fig. 7 should be included in text rather in figure caption, too. In Figure 7 the data and polynomial fits of Eqs. (3) should be shown (e.g. scatter plots of sideslip angle against k_β for one small and one large attack angle) to get an idea of the sensitivity (non-linearity) to noise and the quality of flow angle measurements at such large flow angles. The panels in Fig. 7 are not very useful. Also, in Fig. 8 the M2AV airspeed is less noisy at high frequencies, but on the other hand some low frequency variations observed in MASC have lower amplitude in M2AV (not necessary at high flow angles). Low frequencies are significant for flux measurements.*
Figure 7 will be replaced by figures 1, 2 and 3 shown below. Figure 1 shows the two dimensionless pressure coefficients k_α and k_β plotted against each other for a full calibration routine. It can be seen that at higher airflow angles, the non-linearity becomes considerably large. In figure 2 and 3 this can also be seen for the correction coefficients for dynamic pressure k_q and for static pressure k_p. Especially angles larger than 10^o are concerned. A 9th order polynomial fit is applied to map the non-linearities to measurements. It can also be seen that k_p has larger non-linearities at smaller angles. In the revised manuscript, this information will be added to the text in chapter 2.2.

It is true that noise on the ring port pressure will effect not only the high frequencies, but the full spectrum. In the extreme case that is shown in figure 8 in the

AMTD
6, C4338–C4350, 2014

discussion paper, this has large effects. In most cases, the critical angles for noise on the ring pressure ports is not met, thus, the effects are smaller. Figures 4 and 5 show such a second flight example. In this case also the effects on the low frequencies are less compared to the extreme example given in the discussion paper. This supports the statement that it is not the different method of probe calibration that causes the errors, but the aerodynamic effects at the ring pressure ports.

3. *Page 9790, lines 25-28: Why differential pressure between the two attack angle holes and the differential pressure two sideslip angle holes are not measured directly and possible with less noise? These are the measurements that are actually used in the derivation of flow angles as the authors state too.*
The measurement of the pressure at each single hole is necessary to calculate ΔP as normalization pressure. A normalization of the calibration makes sense to gain robustness against variations in airspeed. Noise at the holes $dP1$ to $dP4$ was not found to be critical.

4. *Fig. 14: The response of the combined filter which is used drops above 10 Hz. Why not use a filter with higher frequency response? Does measurement noise starts at frequencies just above 10 Hz? Is this limit too low for the purposes of the system (measurement of small scale turbulence)?*
In general, with the methods that were shown in the paper, considerations can be made to increase sampling rate, filter cut-off frequencies and thus frequency response of the system. As also mentioned in the review, the benchmark for airborne turbulence measurements up to date is still between 10 Hz and 30 Hz. As shown, many of these benchmark systems however, can still be further developed to decrease uncertainties and errors. A major reason why higher frequency ranges were not targeted in the system design from the beginning is that the complementary sensors for the wind calculation, i.e. the inertial navigation system (INS), are not capable to provide higher sampling rates than 100 Hz.

AMTD
6, C4338–C4350, 2014

5. *Page 9797, line 22: Correct the double full stop.*
   This will be corrected in the revised manuscript.

6. *Fig. 15: The authors should fit the inertial subrange lines to each spectrum (or structure function) to have a more clear view of the frequency (or time lag) where it departs from the expected isotropic behavior. The expected entry point of the inertial subrange should be indicated, too. Obviously, more examples are needed (or a composite normalized spectrum) to have a definite conclusion on the improved behavior of M2AV over MASC.*

   The Kolmogorov slopes were fit to the MASC and the M^2AV curve independently now. Additionally, the MASC curves were shifted to lower powers in the plots to improve the readability. The entry point of the inertial subrange is in both cases visually found at about 1 Hz (time lag of 1 s). Calculating the integral length scale Λ for each individual flight leg and averaging the result returns 27 m for the flight with MASC and 39 m for the flight with the M^2AV. Scaling Λ with the airspeed of the aircraft yields the integral time scale, which is about 1.1 s for the MASC flight and about 1.5 s for the M^2AV flight. This fits well with the visually determined start of the inertial subrange just below the corresponding frequencies. It is indicated by dashed lines in the plot (figure 6 and 7). It has to benoted though, that true airspeed is not a meteorological variable (as also mentioned by referee #1) and thus, the entry point of the inertial subrange and the integral length scale that are calculated here are not actual meteorological quantities.

   More then one flight was analysed for the comparison between M^2AV and MASC (see answers to referee #1). The consistent improved behaviour of the MASC system was depicted by one representative example to give the reader an idea about the current state of the art.

7. *Page 9799, lines 10-11: Flow distortion by the aircraft parts is a crucial issue.*

AMTD
6, C4338–C4350, 2014

Some related references could be included by the authors, as they did for wind calculation equations in the next sentence.
References to the articles Crawford et al. (1996) and Wyngaard et al. (1985) will be given in a revised manuscript at this point. These articles give a detailed insight into the issues of flow distortion, the causes and quantification of the effects and possible correction methods.

References

Crawford, T. L., Dobosy, R. J., and Dumas, E. J.: Aircraft Wind Measurement Considering Lift-Induced Upwash, Boundary-Layer Meteorol., 80, 79–94, 1996.
Wyngaard, J. C., Rockwell, L., and Friehe, C. A.: Errors in the Measurement of Turbulence Upstream of an Axisymmetric Body, J. Atmos. Oceanic Technol., 2, 605–614, 1985.

Interactive comment on Atmos. Meas. Tech. Discuss., 6, 9783, 2013.

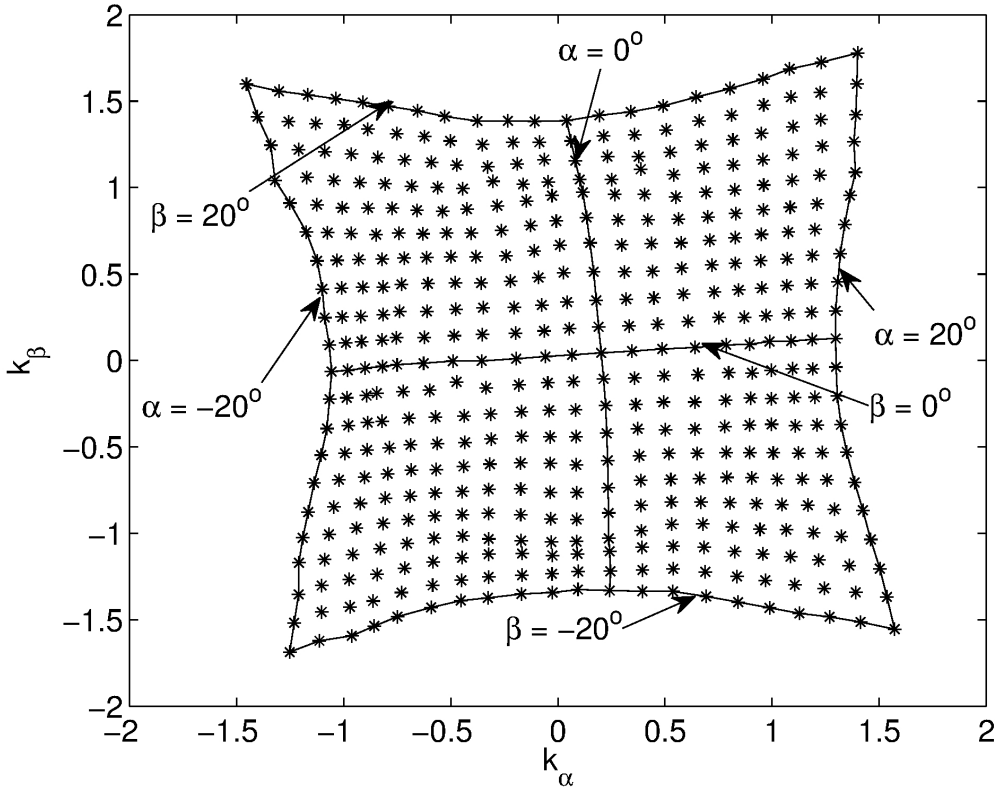

Fig. 1. Two dimensional plot of k_β over k_α. The figure shows the nonlinearities that are larger for higher airflow angles α and β.

AMTD
6, C4338–C4350, 2014

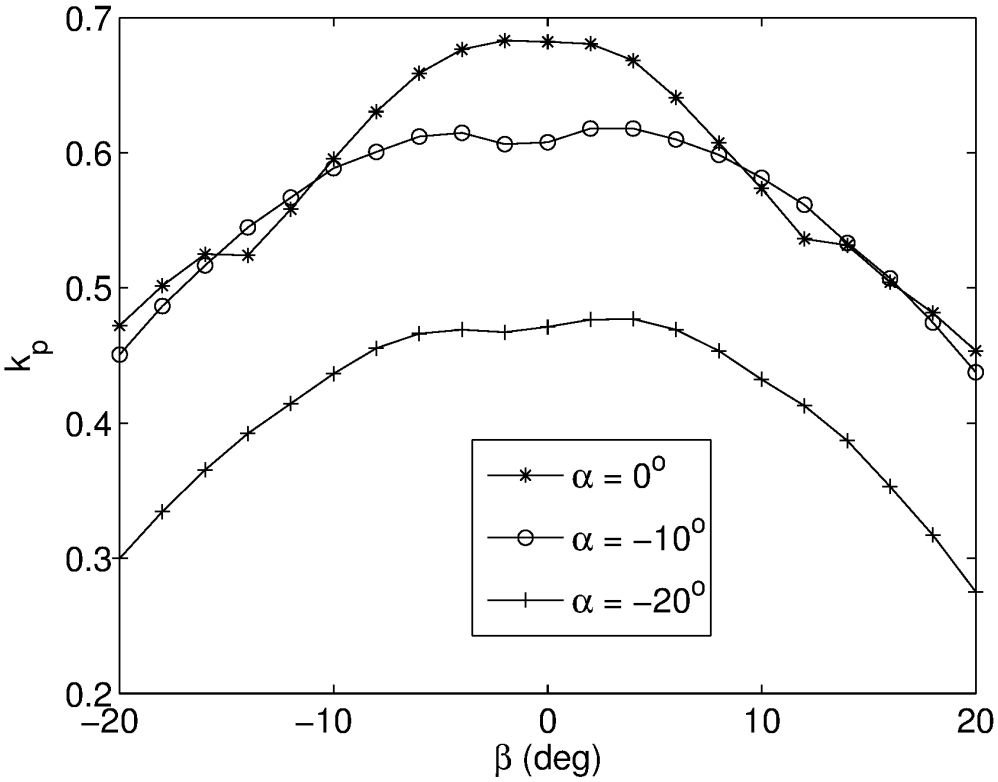

Fig. 2. Calibration coefficient k_p for static pressure plotted against calibration angle β for three attack angles α.

AMTD
6, C4338–C4350, 2014

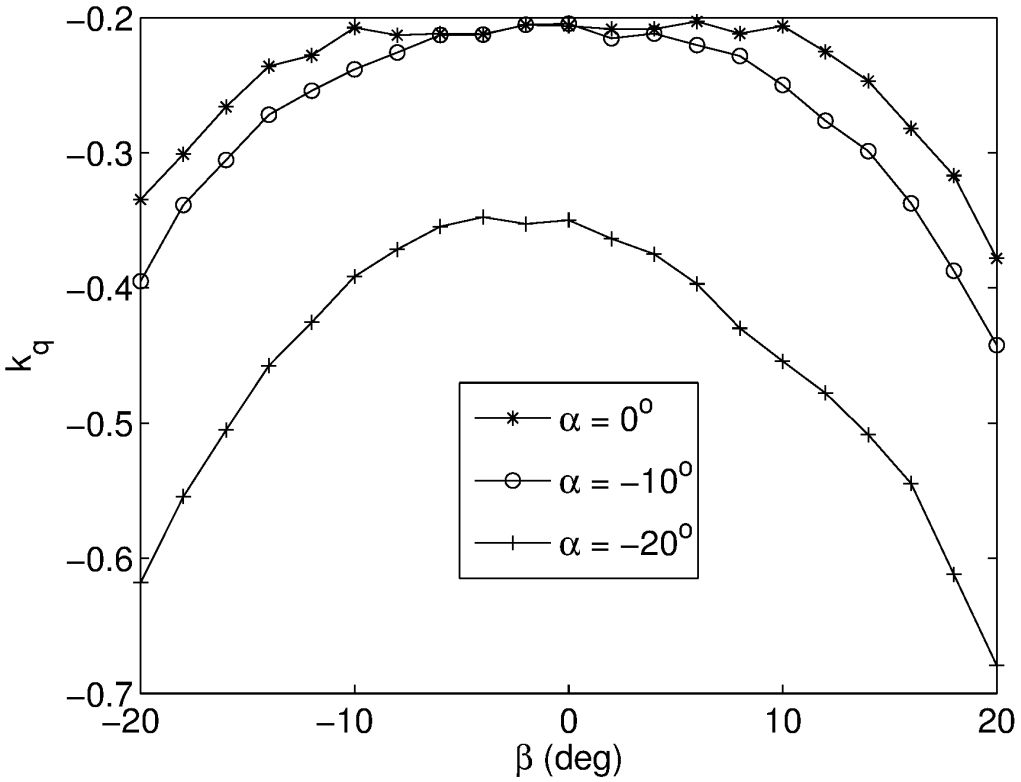

Fig. 3. Calibration coefficient k_q for dynamic pressure plotted against calibration angle β for three attack angles α.

AMTD
6, C4338–C4350, 2014

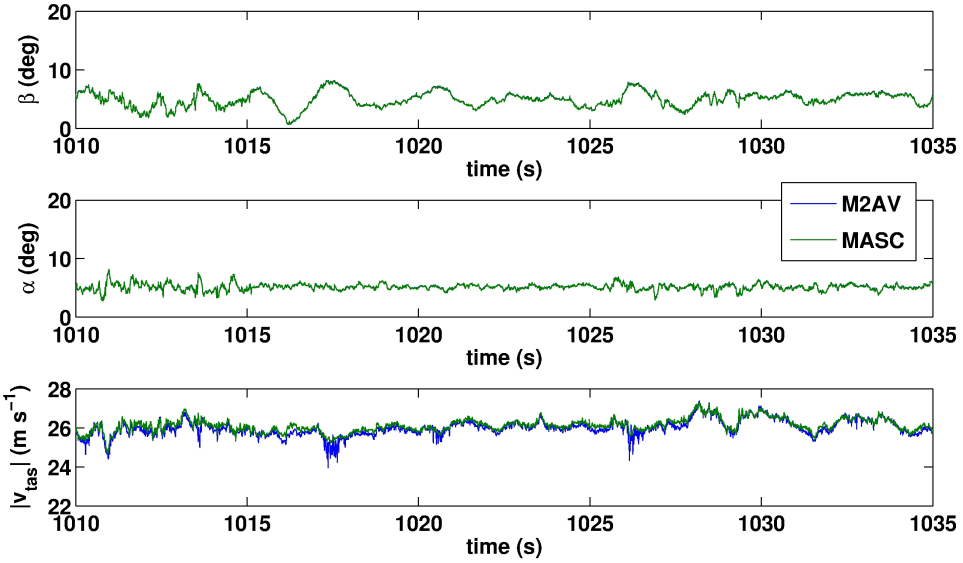

Fig. 4. Airflow angles and true airspeed, measured with the five hole probe and calculated with the $\rm Mˆ2AV$ method, and the MASC method respectively.

Full Screen / Esc
Printer-friendly Version
Interactive Discussion
Discussion Paper

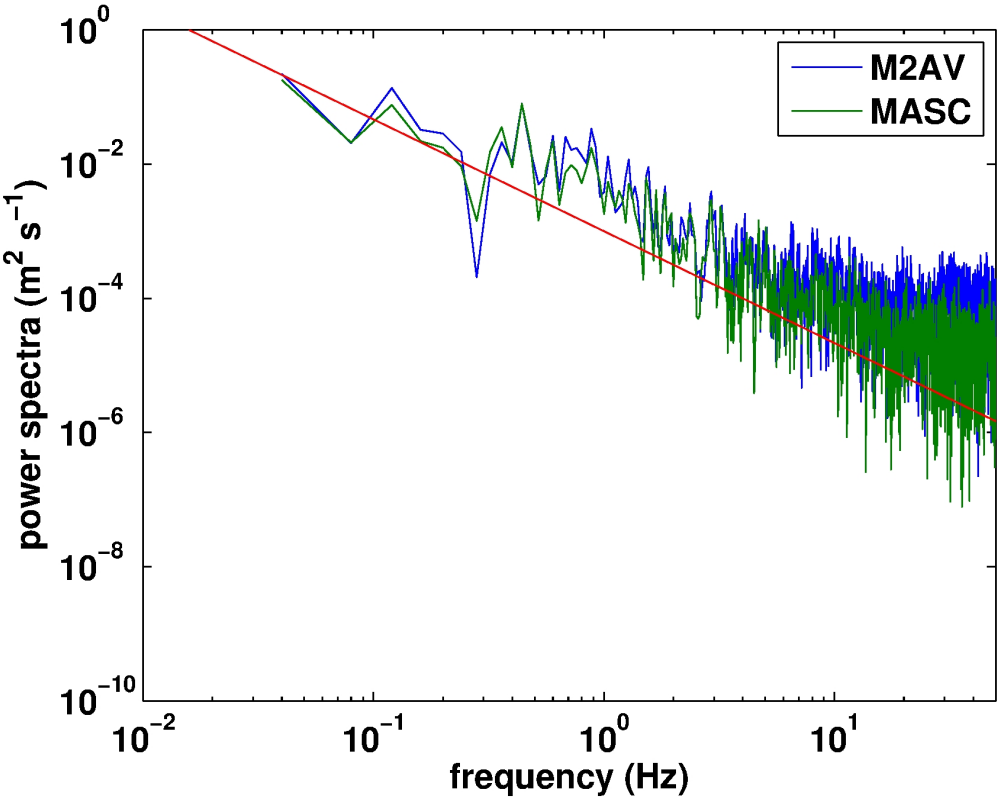

Fig. 5. Spectra of the true airspeed measurement in flight with $\rm Mˆ2AV$ method, and the MASC method respectively. The red line shows the $kˆ{-\frac{5}{3}}$ slope.

AMTD
6, C4338–C4350, 2014

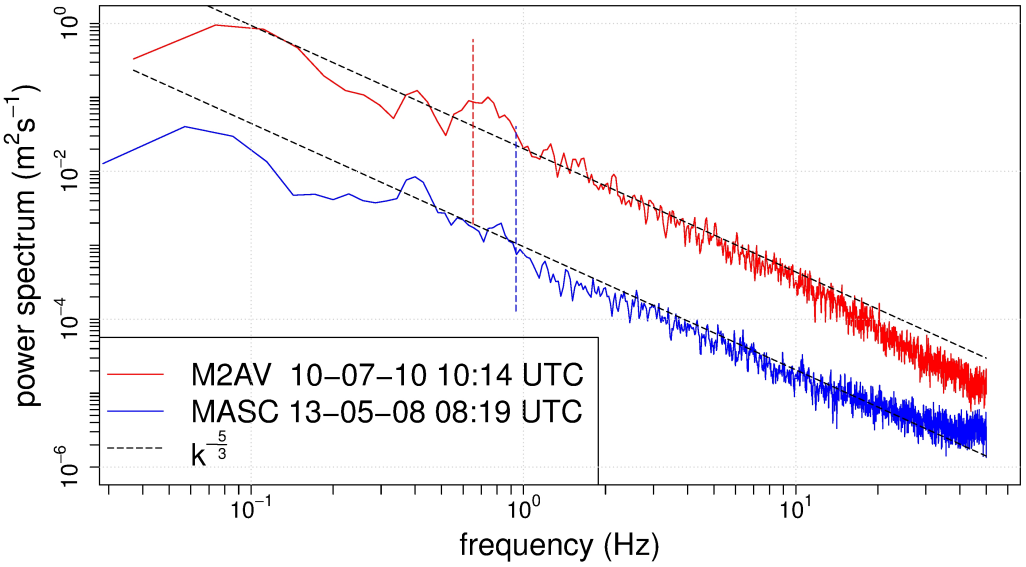

Fig. 6. A variance spectrum of true airspeed measured with the MASC RPA in comparison to a measurement with the $\rm M^2AV$ RPA.

AMTD

6, C4338–C4350, 2014

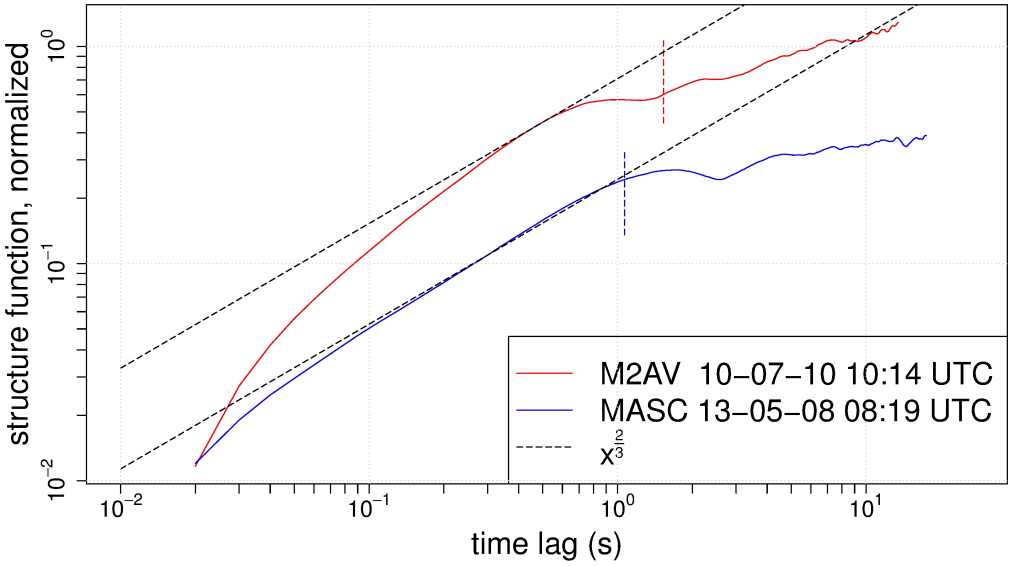

Fig. 7. A structure function of true airspeed measured with the MASC RPA in comparison to a measurement with the $\rm Mˆ2AV$ RPA.

AMTD
6, C4338–C4350, 2014